



PERGAMON

Deep-Sea Research II 50 (2003) 2371–2388

---

---

DEEP-SEA RESEARCH  
PART II

---

---

www.elsevier.com/locate/dsr2

# Seasonal dynamics of the surface circulation in the Southern California Current System

Emanuele Di Lorenzo\*

*Scripps Institution of Oceanography, University of California, San Diego, La Jolla 92093-0224, USA*

Received 6 May 2002; received in revised form 10 October 2002; accepted 1 November 2002

---

## Abstract

The seasonal dynamics of the Southern California Current (SCC) is investigated using a primitive equation ocean model with real coastlines and topography. The model is tested with different wind forcing, and the resulting flow fields are compared to the mean and seasonal circulation inferred from long-term in situ observations (California Cooperative Oceanic Fisheries Investigation (CalCOFI)). The model integration forced with the output winds of a regional atmospheric model (RSM) best captures the statistics of the observed circulation, with a 0.9 correlation coefficient for the streamlines and 0.5 for the velocity fields. The model integrations reveal a pronounced linear response of the flow field to changes in winds on the shelf region.

A dynamical feature inferred from CalCOFI hydrography, also suggested in TOPEX/ERS maps, is an annually recurrent westward propagation of SSH anomalies originated in the Southern California Bight (SCB) during the upwelling season. The RSM integration is the only one to capture the correct timing and spatial evolution of this process. We therefore use this model integration for guidance in constructing a dynamical framework to interpret the observed circulation and its variability.

During the upwelling season in spring, there is an upward tilt of the isopycnals along the coast directly forced by the winds in the Bight. As the spring transitions to the summer the upwelling winds relax in the Bight but are still strong in the region offshore, approximately in correspondence of the continental slope (positive wind-stress curl condition). Anomalous denser waters in the location of the Southern California Eddy are maintained and reinforced by the combined interaction of the coastal/islands geometry and the wind-stress curl (through Ekman dynamics). The adjustment process to the denser water initiates a westward propagation of ocean density anomaly through Rossby waves, and reinforces the cyclonic gyre-like circulation of the SCE (increasing positive vorticity). Surface poleward flow, maintained by the positive wind-stress curl, is also reinforced in proximity of Point Conception as a consequence of the adjustment. During the summer the cyclonic gyre becomes increasingly unstable as the core of the ocean anomalies crosses the continental slope. Instability processes within the cyclonic region, characterized by a sharp increase in EKE, shed eddies that leave the region either drifting to the west or interacting with existing eddies in the region offshore. The EKE reaches a seasonal maximum at the end the summer in the cyclonic region, and in late fall further offshore where the eddies are fully developed.

The shedding of eddies cannot be directly seen in the CalCOFI observations because of the sampling aliasing. For this point we rely on the strong suggestion of the model, which we assume is able to capture the leading order dynamics. Additional integrations with a linearized version of the model are also presented to reinforce

---

\*Tel.: +1-858-534-6397; fax: +1-858-534-8561.

E-mail address: edl@ucsd.edu (E. Di Lorenzo).

our interpretation of the westward propagation of the isopycnal anomalous displacement associated with Rossby wave dynamics.

© 2003 Elsevier Ltd. All rights reserved.

*Keywords:* California current; Southern California Bight; Coastal upwelling; Wind-stress curl

---

## 1. Introduction

The southern component of the California Current System (SCCS, here defined as south of Point Conception) was first described in an early report by Sverdrup and Fleming (1941). In their study based on ship cruise measurements, they isolated three circulation features: an offshore equatorward alongshore current (California Current, CC), a surface Inshore Countercurrent (IC) directed poleward along the coast, and a northward undercurrent (California Undercurrent, CU) over the continental slope at a depth of 200 m. Because the IC does not always flow continuously around Point Conception, the recirculation feature that includes the inshore poleward current in the Southern California Bight (SCB) and the offshore equatorward current has been referred to as the Southern California Eddy (SCE; Schwartzlose, 1963).

In 1949, following the effort of Sverdrup, the California Cooperative Oceanic Fisheries Investigation (CalCOFI) began a routine sampling program of the physical and biological properties of the ocean off Central and Southern California at seasonal resolution. The program is still active today and observational studies make use of these hydrographic measurements to describe the seasonal and interannual variations of the circulation patterns in the SCCS (Lynn and Simpson, 1987; Hayward et al., 1994; Bograd et al., 2000).

Although CalCOFI provides an unprecedented timeseries of oceanographic data, the coarse spatial (80 km), and temporal (3 month) resolution of the sampling array leaves us with an incomplete understanding of the rich mesoscale oceanic structure that is more evident in satellite and drifter observations (Miller et al., 1999; Simpson and Lynn, 1990; Strub and James, 2000; Swenson and Niiler, 1996). The effect of these mesoscale features on the variability of the mean and

seasonal circulation is yet to be fully determined. Simplified numerical ocean models of the California Current System (CCS) isolate several physical processes as potential candidates in generating the observed variability (Auad et al., 1991; Batteen, 1997; Haidvogel et al., 1991; Paressierra and O'Brien, 1989; Paressierra et al., 1993), but the nature of these experiments does not allow for a quantitative assessment of the dominant physical processes of the real system. More sophisticated numerical models that incorporate realistic representation of the intricate California coastline and the outstanding topographic features (Marchesio et al., 2003) can allow a more quantitative analysis of the CCS dynamics. These simulations generate realistic levels of variability along most of the US West Coast (USWC) north of Point Conception but poorly capture the statistics of the flow in the SCCS.

In the SCB, both the geometry and the circulation patterns differ dramatically from the ones north of Point Conception (Hickey, 1992). Very close to the coast, the spatial and temporal characteristic of the currents depend on the local surface winds (Allen, 1980). Regional winds that retain the effects of smaller scale coastal orography have not yet been included as forcing functions in numerical simulations of the circulation in the SCCS.

The objective of this study is to quantify the dominant physical processes that characterize the seasonal dynamics in the SCCS by using an ocean primitive equation model. Different available wind products, both from regional and large-scale analysis, are used to force the model and the results are compared with the 50-year CalCOFI in situ observations. It is shown that the use of regional winds is critical to resolve the spatial and temporal patterns of the circulation. On the shelf, the dominant signal of oceanic seasonal variability is associated with a quasi-linear response of the

currents to changes in the winds. Off the continental shelf the variability is associated with ocean intrinsic variability characterized by a strong eddy field with energy spread over a broad frequency range.

A dynamical framework of the seasonal dynamics in the SCCS based on the model experiments validated with observations is provided. Important elements of the dynamics isolated in this study are: (a) the role of Ekman Pumping in intensifying the SCE, (b) the timing of the seasonal cycle of the currents associated with westward propagation of ocean anomalies from the SCB, and (c) the generation of eddies over the continental slope through barotropic and baroclinic instability.

We proceed now in introducing the model and data (2), comparisons of the mean and seasonal circulation of the model runs with observations (3), a linearized version of the ocean model to investigate the role of quasi-linear Rossby waves in the westward propagation of ocean anomalies from the SCB (4), the relationship between the winds and the current (5), and a dynamical framework of the SCCS to summarize the results (6).

## 2. Model, data and experiment setup

We use an eddy-resolving primitive equation ocean model called the Regional Ocean Modeling System (ROMS), a descendent of SCRUM (Song and Haidvogel, 1994). The model uses a generalized stretched-coordinate system in the vertical and a curvilinear horizontal grid (9 km resolution) that extends about 1200 km along the USWC from northern Baja to north of San Francisco Bay with roughly 1000 km offshore extent normal to the coast (Fig. 1). The vertical grid has 20 levels with enhanced resolution in the surface and bottom boundary layer. The model bathymetry is obtained by a smooth interpolation of the ETOPO5 analysis (NGDC, 1998) and is characterized by an extended (about 150–200 km) continental shelf in the SCB followed by a steep continental slope offshore.

A modified radiation condition (Marchesiello et al., 2001), which allows for stable, long-term

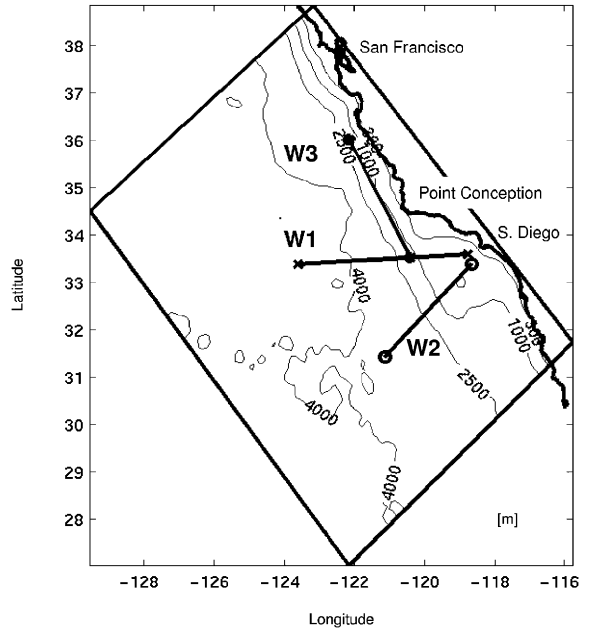


Fig. 1. Model domain, coast line and bathymetry (m). Superimposed W1 westward transect, W2 crossshore transect and W3 northward transect following topographic slope.

integration of the model, is used at the three open boundaries together with a nudging term for relaxation to observed climatologies. The nudging is stronger (timescale of 1 day) if the direction of the flow is inward and weaker (timescale of 1 year) for the outflow. Marchesiello et al. (2003) have successfully used the model in this configuration to study the long-term equilibrium structures of the CC over the entire USWC. A more complete report of the model numerics, open boundary conditions and mixed layer parameterizations can be found in Shchepetkin and McWilliams (1998, 2003) and Large et al. (1994).

For the model initial condition and open boundaries we use the Levitus et al. (1994) temperature ( $T$ ) and salinity ( $S$ ) monthly climatologies. At the surface, the model is forced with monthly climatologies for heat and freshwater flux derived from COADS (da Silva et al., 1994). Different monthly wind-stress climatologies are used to test the model as follows.

### 2.1. RSM case

The wind stress is obtained by averaging the daily output of a regional atmospheric model (RSM) of Southern California to form monthly climatologies. The atmospheric regional model is part of the Experimental Climate Prediction Center (ECPC) forecasting system (<http://ecpc.ucsd.edu>) and is used to downscale daily global NCEP analyses. The data available from the ECPC runs, is from 1997 to present. Building a monthly climatology with this shorter time series is questionable, since we only have five realizations for each month. Nevertheless, during this time frame the system experienced both normal years and El Niño/La Niña events so that we can fairly assume that the mean monthly conditions will not be biased towards any of these states.

### 2.2. COADS case

Monthly climatologies of wind stress at  $2 \times 2$  degree resolution have been downloaded from the Climate Diagnostics Center (CDC) website (<http://www.cdc.noaa.gov>) and interpolated to the model grid. These winds are the same winds used by Marchesiello et al. (2003). The COADS at  $1 \times 1$  degree resolution did not show a well-defined seasonal cycle in the SCB so the model results from this integration will not be presented.

### 2.3. NCEP Pacific Ocean Analysis case

Monthly means (1980–present) of wind stress at  $1 \times 1.5$  degree resolution were interpolated to the model grid. The NCEP Pacific Ocean Analysis data are provided by CDC (<http://www.cdc.noaa.gov>).

### 2.4. The CalCOFI dataset

The observations we are trying to interpret are 50 years (1949–present) of T and S CTD data collected from cruises by the California Cooperative Oceanic Fisheries Investigations (CalCOFI; <http://www-mrlg.ucsd.edu/calcofi.html>). The data have monthly resolution for the first 15 years and then vary from monthly to seasonal (four cruises

per year). To compare the dataset with model runs we binned the cruises by month and objectively analyzed the data at standard depth from the surface to 500 m depth.

## 3. The Southern California Current System: observations and model experimental results

In order to assess which model integration yields a better understanding of the physical processes that characterize the mean and seasonal variation of the SCCS, a comparison with observations is required. Our goal is to show that the model captures the leading order dynamics of the observed system when driven by adequately realistic atmospheric forcing. A rigorous quantitative measure of the model's skill in capturing the dynamics of the system based on individual synoptic observations is addressed in a different study by Di Lorenzo et al. (2003).

### 3.1. The mean

The CCS in Southern California between 29 and 36N, inferred from the CalCOFI hydrography, is described in the literature in terms of four distinct features: an offshore equatorward flow (CC) located approximately 300 km from the coast, an inshore surface (IC) and sub-surface (CU) poleward flow, and a region of cyclonic circulation (SCE) that connects the inshore and the offshore circulation (Chereskin and Trunnell, 1996; Lynn and Simpson, 1987). The mean circulation from CalCOFI hydrography is represented in Fig. 2a as the depth  $h$  of the density surface  $\sigma = 26.5$ , which approximately corresponds to the interfacial depth of the first baroclinic mode. The main circulation patterns in this map are now compared to those obtained by integrating the model with different wind forcing.

#### 3.1.1. California current

Offshore equatorward flow in CalCOFI observations is found in all seasons (Fig. 3) and thus appears as a strong signal in the annual mean circulation (Fig. 2a). The model experiments all capture this equatorward flow (Fig. 2). The pattern

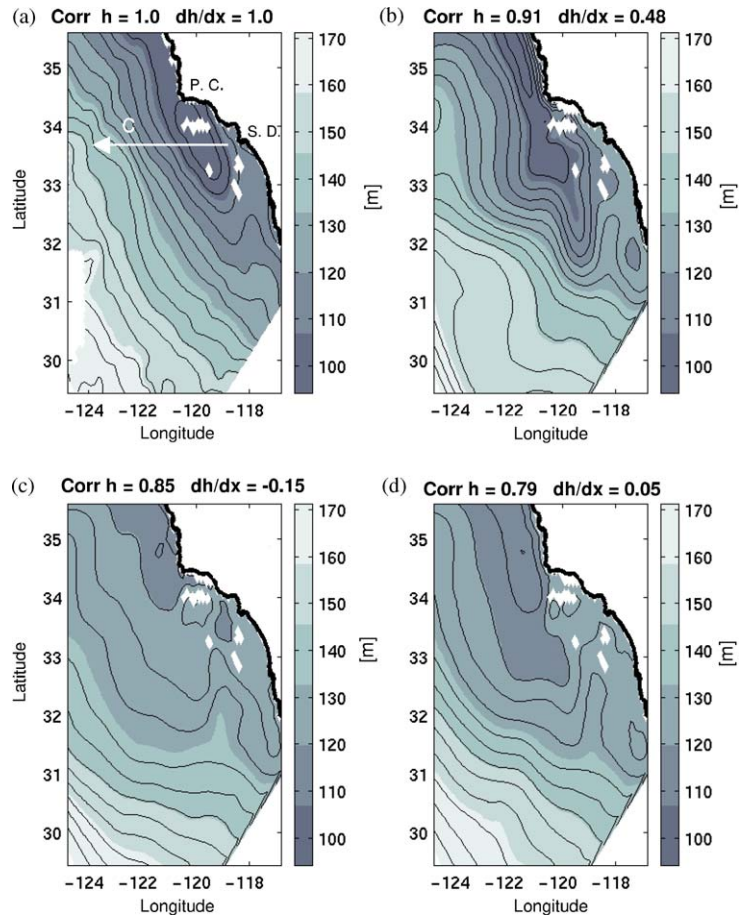


Fig. 2. Mean depth  $h$  of the 26.5 isopycnal (a) from CalCOFI observations compared to the one obtained by integrating the model with the (b) RSM winds, (c) COADS  $2 \times 2$ , and (d) NCEP Pacific Ocean Analysis. On the top correlation coefficient (against the observation in a) for the depth  $h$  and zonal gradient  $dh/dx$ .

correlation coefficient (Corr.) with CalCOFI (Fig. 2a) is 0.9 in RSM (Fig. 2b), 0.79 in NCEP (Fig. 2d) and 0.85 in COADS (Fig. 2c). A more stringent test of verisimilitude is to compare the gradient of the interfacial height ( $\approx dh/dx$ ) which is a proxy for the geostrophic flow at that level. The alongshore geostrophic flow associated with the core of the CC does not correlate well with the observed. In cases COADS and NCEP, the flow is much weaker than in CalCOFI and the spatial structure is broader (correlations near zero). The strength of the flow in case RSM is more comparable to CalCOFI than either other case, and the pattern correlation is relatively high (Corr. = 0.48).

### 3.1.2. Inshore Countercurrent (IC)

Poleward inshore coastal flow in the observations is characterized by pronounced seasonal variability in the SCB, stronger in the summer and almost zero in spring (Fig. 3). In the mean it appears as the inshore components of the SCE (Fig. 2a). In cases COADS (Fig. 2c) and NCEP (Fig. 2d), a clear expression of inshore poleward flow in the Bight cannot be found. On the contrary, case RSM shows a strong poleward flow that extends from the Bight to north of Point Conception. A qualitative explanation for the differences in the model experiments is associated with the different patterns of the mean wind-stress curl in the Bight. Studies by Oey (1999) and

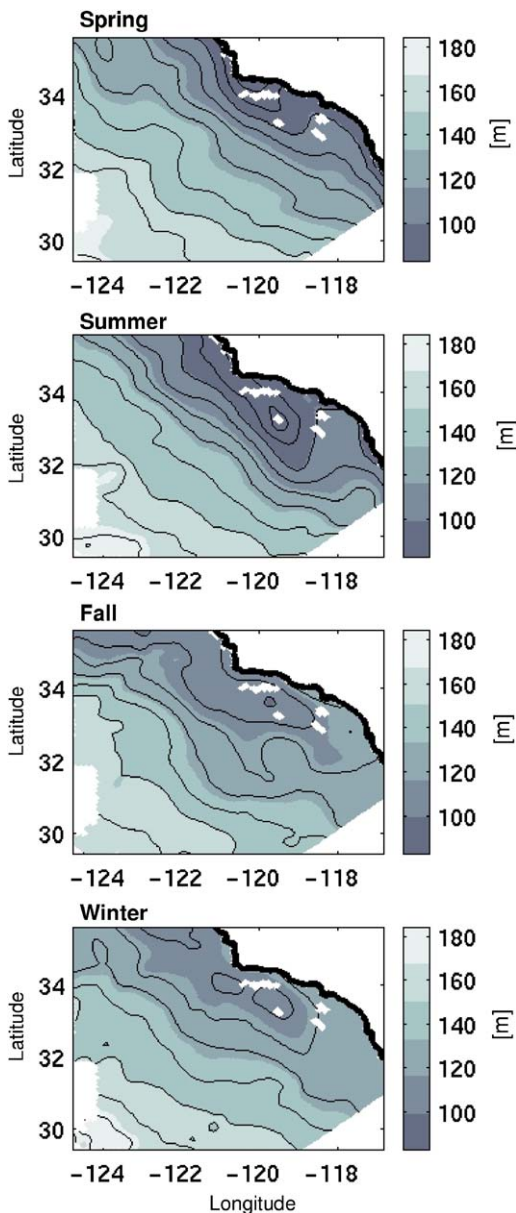


Fig. 3. Mean depth  $h$  of the 26.5 isopycnal from CalCOFI observations for the seasons of spring, summer, fall and winter. Contour interval is 10 m.

McCreary et al. (1987) suggest that the forcing mechanisms of the poleward flow rely on positive wind-stress curl and its alongshore gradient. NCEP (Fig. 4d) and COADS (Fig. 4c) wind stresses have a weak or almost zero curl along

the coast in the Bight, therefore missing these forcing mechanisms. In RSM winds, the region of positive wind-stress curl is well defined and strong in the coastal shelf region, supporting the idea of a relationship between curl of the winds and poleward flow in the SCB. A more detailed discussion of the dynamics of this poleward flow and its vertical structure, as inferred by the ocean model experiments of this study will be addressed in a later paper by Di Lorenzo et al.

### 3.1.3. Southern California Eddy (SCE)

The cyclonic gyre-like circulation south of Point Conception is a prominent feature in mean dynamic-height maps from CalCOFI hydrography. On seasonal timescales, the SCE is better described as a region of recirculation with offshore equatorward flow and inshore poleward flow rather than a closed eddy. Indeed, a closed gyre, with structure resembling this mean flow, cannot be identified in any of the individual CalCOFI synoptic maps or in the more recent ADCP current analyses (Bray et al., 1999). The strength of this recirculation has a clear seasonal cycle being strongest in the summer when the IC has its seasonal maximum (Lynn and Simpson, 1987) and almost zero during the upwelling season in spring-time.

Case COADS (Fig. 2c) is clearly unable to capture the spatial pattern of this recirculation region. Case NCEP has a weak and offshore signature of the recirculation. Only case RSM (Fig. 2b) has a strong and nearshore recirculation as observed in CalCOFI.

Mean wind-stress curl maps of the different forcing (Fig. 4) show a strong local correlation between the positive wind curl and the location of the model SCE recirculation. In case RSM, the positive wind-stress curl is very strong and close to shore as is the recirculation. In case NCEP, the recirculation (Fig. 2d) pattern is farther offshore and tracks the offshore region of positive wind-stress curl (Fig. 4d). In case COADS, there occurs no region of positive wind-stress curl at the coast (Fig. 4c) and no clear recirculation.

We note that the region of maximum positive wind-stress curl in case RSM is not as far inshore as that of the product derived by Winant and

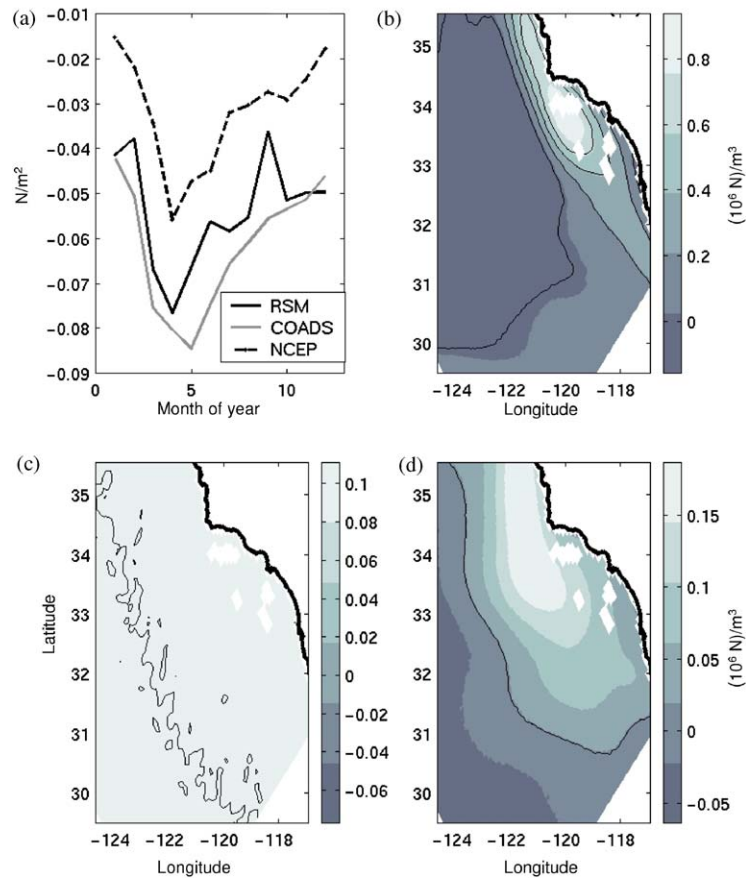


Fig. 4. (a) Seasonal cycle of alongshore winds averaged over model domain (negative is towards the south) for the three different cases. Mean wind stress curl of (b) RSM winds, (c) COADS  $2 \times 2$ , and (d) NCEP Pacific Ocean Analysis. The color bars are different on each panel in order to better show the contours.

Dorman (1997) from buoy winds in the SCB which show a strong peak in the Santa Barbara Channel. The SCE, and its dynamics, can be further understood in the context of the seasonal cycle which we address in the next section.

### 3.2. The seasonal cycle

Although characterizing the mean circulation in a schematic way is useful and has been adopted by most authors when describing the Southern component of the California Current System (SCC) (Chereskin and Trunnell, 1996; Hickey, 1998; Lynn and Simpson, 1987), it is also important to recognize that any given synoptic map will hardly resemble this schematic picture.

Satellite observations of SST and SSH have revealed a variety of mesoscale features such as cold filaments (Strub et al., 1991) and mushroom shaped SST patterns (Mied et al., 1991) associated with the strong eddy field.

Strub and James (2000) suggested that the primary source of energy for these eddies is the potential energy of a density front in proximity of the coast generated by the upwelling winds in spring. They characterized the seasonal cycle of EKE in the context of the seasonal wind variations along the coast of California as follows: (a) An equatorward coastal jet develops along the coast in spring with the strong upwelling winds. (b) The jet undergoes westward displacement, during spring and summer, away from the coast likely associated

with Rossby wave dynamics. (c) During this offshore propagation, dynamical instabilities associated with the jet and with baroclinic energy conversion from the density front are the generating mechanism of the eddies and meanders of the CC. (d) Along the coast a surface poleward flow develops and intensifies during summer and fall. (e) In winter and early spring the jet has dissipated its energy and a weaker equatorward flow is typically found in the offshore waters. The cycle

starts again with the new upwelling winds in the following spring.

A prominent and important component of the seasonal cycle, as depicted by Strub and James, is the westward propagation. Kelly et al. (1998) documented a region of maximum EKE migrating westward on seasonal timescales associated with instabilities in the core of the CC.

The CalCOFI hydrography (Fig. 6) and the 10-day average TOPEX/ERS maps (Fig. 5) also

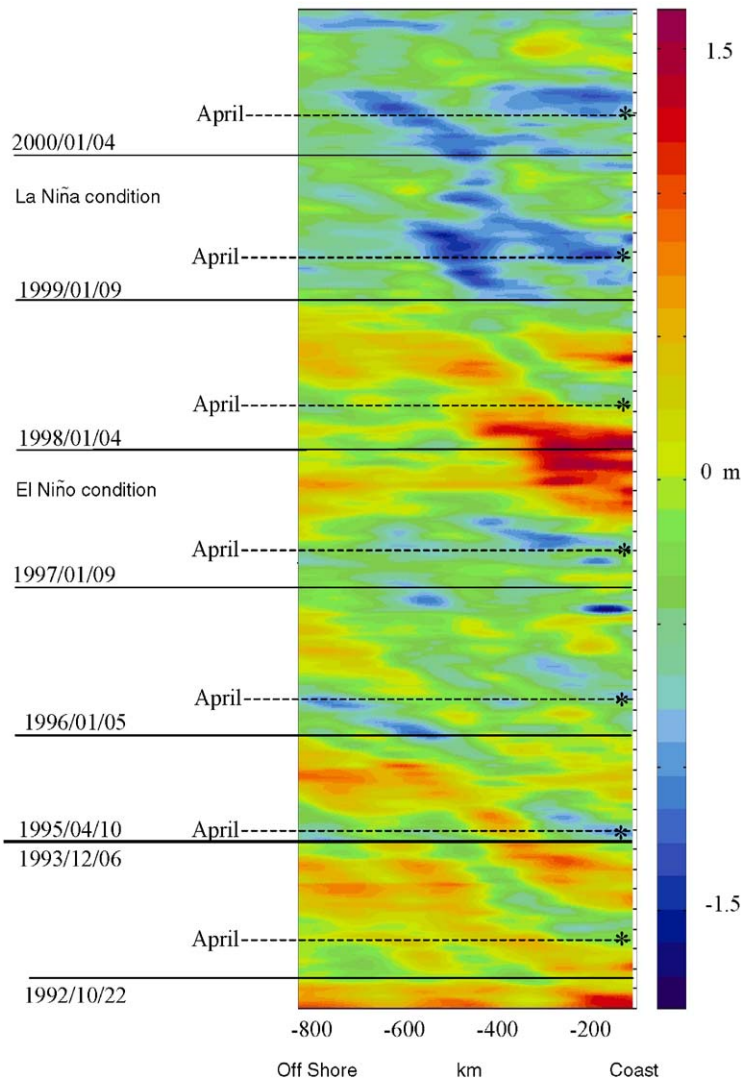


Fig. 5. Hovmoeller plots of SSH anomalies from TOPEX/ERS 10-day maps averaged alongshore.

suggest an annually recurrent westward propagation of SSH anomalies that originated in the SCB during the upwelling season. The kinematics differ from that described by Strub and James (2000) because of the complex geometry and forcing in the SCB, but the general character is similar. We therefore seek the signature of this dynamical feature in the model integrations as a qualitative measure of the ability of the different winds to generate the seasonal cycle with the correct time and space signature.

For the model-data comparison we choose the east–west transect W1 (Fig. 1) of the anomalous depth  $h$  of the density layer 26.5, plotted as a function of the month of the year (Fig. 6). The first element common to all of the model integrations and the observations is the signature of the upwelling winds in April. This can be seen as the shoaling of the density layer at the coast (dark negative values to the right in all panels of Fig. 6). As we progress towards the summer, cases COADS (Fig. 6c) and NCEP (Fig. 6d) show a clear westward propagation of the disturbances that originated at the coast. In CalCOFI (Fig. 6a) the disturbance develops throughout the spring and early summer over the entire shelf region in contrast to cases NCEP and COADS in which the disturbances develop only in a very narrow coastal band. Furthermore, the westward propagation in CalCOFI (Fig. 6a), only occurs offshore of the shelf region with a maximum at the end of the summer (from arrow a to arrow b in 6a). Although the phase speed of the disturbances in cases COADS and NCEP is comparable with the observations (arrow b in Fig. 6a, c and d), the spatial development of these anomalies and their path is not captured. We therefore conclude that these two wind forcing datasets are inadequate to investigate the seasonal dynamics of the Southern California Current System.

We now focus our attention on the RSM (Fig. 6b) experiment. We first note that the pattern correlation coefficient with CalCOFI (0.73) is significantly higher than in cases COADS (Fig. 6c) and NCEP (Fig. 6d). The development of the seasonal anomaly occurs over the entire shelf region as observed in CalCOFI and the propaga-

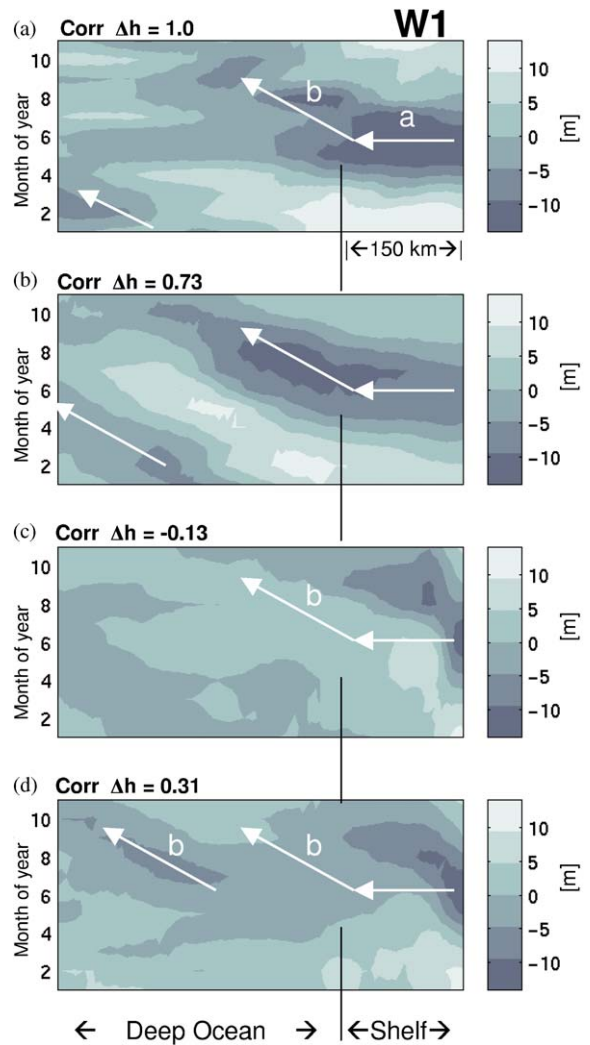


Fig. 6. Westward transect W1 ( $x$ -axis) of the mean 26.5 isopycnal depth anomaly ( $\Delta h$ ) as a function of month of the year ( $y$ -axis): (a) CalCOFI observations, (b) case RSM winds, (c) case COADS  $2 \times 2$ , and (d) case NCEP Pacific Ocean Analysis. Correlation coefficients with (a) are plotted in the top left corner of each panel.

tion path (arrow a and b in Fig. 6) is comparable with the observed as well.

The timing and spatial distribution of the anomaly in case RSM seems to be associated with the seasonal development of stronger positive wind-stress curl over the entire shelf region during the upwelling season (April, Fig. 7a). This positive wind-stress curl pattern persists and intensifies

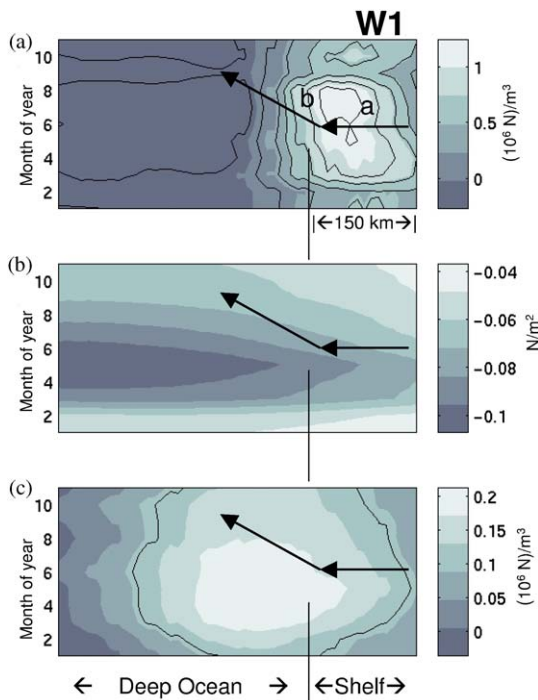


Fig. 7. Same transect as Fig. 6, but now plotted are the (b) RSM wind-stress curl, (c) COADS  $2 \times 2$  alongshore component of the winds, and (d) NCEP Pacific Ocean Analysis wind stress curl. Please note that (c) is wind stress and not wind-stress curl.

during the summer over the shelf in the RSM wind product and is consistent with observational studies (Bakun and Nelson, 1991; Winant and Dorman, 1997), although the exact spatial pattern and amplitude are still a matter of discussion. The mean wind-stress curl spatial pattern in the RSM product (Fig. 4b) has maximum curl further offshore than the observed (from Winant and Dorman, 1997) and has amplitude that is 25% smaller.

Before ending this section it is useful to investigate the relationship between wind forcing and the oceanic depth anomaly in cases NCEP and COADS as a measure of the sensitivity of the circulation to changes in the winds. In case NCEP, the positive wind-stress curl is located offshore (Fig. 7c) and it forces a westward propagating depth anomaly in the deeper ocean (Fig. 6d). This offshore pulse is independent of the one generated in the near coastal region (Fig. 6d) from the

upwelling winds. The Rossby wave response to Ekman pumping in the California offshore waters has been previously suggested by Kelly et al. (1993). In case COADS, the upwelling favorable winds generate a depth anomaly only along the coast (Fig. 6d). The wind-stress curl in COADS is so weak that we only plot a transect of the alongshore component of the wind stress in Fig. 7c.

In summary we suggest that the seasonal development of the ocean anomaly in the bight is strongly controlled by both the alongshore winds (coastal upwelling) and the positive wind-stress curl acting over the entire shelf region (Ekman pumping) between spring and summer. The westward propagation of the ocean anomaly from the continental shelf cannot be explained in terms of wind forcing alone, but requires an understanding of the dynamical response of the ocean. A more careful analysis of the dynamics is provided in the following sections under the assumption that the ocean model forced with the RSM winds captures the leading order seasonal dynamics of the system and therefore can be used as a guide.

#### 4. Linearized dynamics and westward propagation

We now attempt to evaluate the extent to which the dynamics of westward propagating disturbances that originate on the shelf region in the SCB can be explained in the framework of quasi-linear long waves forced by the wind. In order to do so we linearize the primitive equation model around a state of rest and force it with the RSM winds. In the linearization we also drop the advection term  $u' \cdot \nabla \bar{\rho}$ . This is motivated by our interest in retaining only the long wave response of the system. Under this assumption, advection appears as a second-order term in the expansions, so that the equation for the perturbation density in the interior to first order becomes

$$\frac{\partial \rho'}{\partial t} + \bar{w} \cdot \frac{\partial \bar{\rho}}{\partial z} \approx 0.$$

We integrate the linearized model for 12 years. No eddies are found in the model results. Each model year shows the same seasonal cycle in which

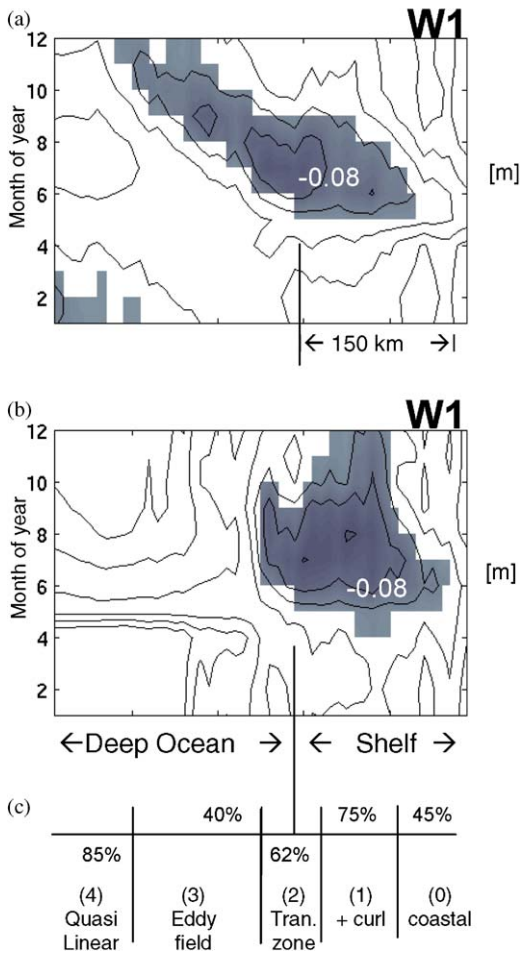


Fig. 8. Westward transect W1 ( $x$ -axis) of SSH anomalies (m) from the linearized model. Dark area is negative and increases towards the white  $CI=0.03$ ). Integrations with (a)  $\beta \neq 0$  and with (b)  $\beta = 0$ . (c) Fraction of variance explained by the linearized model when compared to the non-linear as a function of cross-shore location. The variable used for the comparison is the depth anomaly of the density surface 26.5.

the dominant variability is associated with the development of SSH anomalies on the shelf region and their westward propagation towards the deep ocean (Fig. 8a). A comparison of this signal with the one in the non-linear RSM integration along the westward transect W1 (Fig. 1), reveals that the linearized model is able to explain up to 80% of the temporal variance of the density surface (26.5) depth anomaly in the region of strongest positive

wind-stress curl (Fig. 7a). In this shelf region the Ekman pumping (through  $w'$  in the perturbation density equation) is the generating mechanism of the density surface depth anomaly. (Note: because we are only resolving the long-wave response of the system, the linearized model is unable to resolve the contribution of upwelling due to the alongshore component of the wind at the coast (Fig. 8c, 0).) As we proceed westward along the transect W1, the explained variance drops to 62% over the continental slope (hereinafter referred to as the *transition zone* Fig. 8c, 2), and 40% further offshore (hereinafter referred to as the *eddy field zone* Fig. 8c, 3). In the *transition* and *eddy field zone* the positive wind-stress curl is now negligible (Fig. 7a) and the explained variance is associated with westward propagating disturbances excited on the shelf.

In order to assess the relative contribution of Rossby wave dynamics controlled by the beta effect versus other types of dynamics, we make an additional integration of the linearized model on the  $f$ -plane. The result of this integration (Fig. 8b) shows the same seasonal development of SSH anomaly in the region of strong positive wind-stress curl but not the westward propagation beyond the continental slope. We therefore are confident that the assumption of quasi-linear Rossby waves to explain the westward propagation is valid. Notice that in the  $f$ -plane case the depth anomaly perturbation on the shelf persists longer throughout the fall.

It is also interesting to note that far from the coast on transect W1 the explained variance associated with the quasi-linear Rossby waves that have successfully propagated to the deeper ocean increases to 85% (Fig. 8c, 4). This suggests that other processes are important in the *eddy field zone* (Fig. 8c, 2 and 3). An energetic analysis of the non-linear RSM integration case suggests that instability processes on the continental slope (Fig. 8c, 2) contribute to increasing the energy of the offshore mesoscale *eddy field zone*, defined as the region of maximum variance of SSH anomalies. The non-linear component of these eddies cannot be captured by the linearized model.

In summary, the linearized model analysis suggests the existence of a shelf region and

*transition zone*, in which the dominant dynamical signal is controlled by a quasi-linear response to the changes in the forcing, an *eddy field zone*, in which the dominant dynamics are non-linear, and a further offshore region (Fig. 8c, 4) where the linear dynamics are recovered. This distinction is

also evident in a spectral analysis of the SSH anomalies in the inshore region (Fig. 9a), defined as the shelf and continental slope, and in the offshore region (Fig. 9b). The linearized model average spectra (black line) in the inshore and offshore region are essentially the same showing a

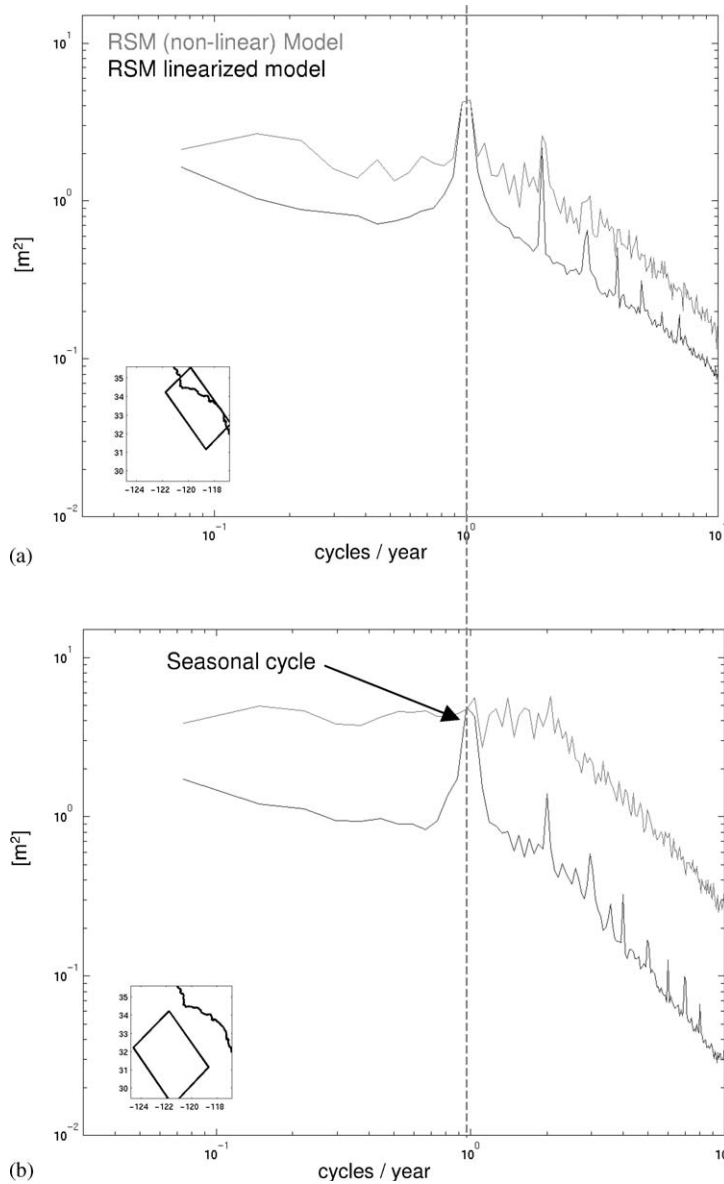


Fig. 9. Average spectra of SSH anomaly (m) for the non-linear and linearized version of the model in the Bight (a) and offshore region (b). The averaging region is shown in the bottom left corner of each panel.

strong peak at the frequency of the seasonal cycle and its harmonics. The same spectral analysis on the non-linear model (gray line) shows similar peaks in the inshore region but noticeable differences in the offshore spectra. In particular, in the offshore region the seasonal peak and its harmonics are no longer separable. The offshore spectral energy in the non-linear case is much higher and spreads uniformly across the seasonal to intra-seasonal frequency band, indicating the presence of the eddy field. It is noteworthy that the energy of the non-linear model is also higher in the inshore region, but not nearly as much as in the offshore.

This analysis suggests that the inshore seasonal circulation can be largely explained by a linear dynamical response of the circulation to the forcing. In the next section we attempt to linearly decompose the forcing and circulation patterns.

## 5. Relationship between the winds and circulation patterns

We have identified that the dominant component of the seasonal variability of the oceanic thermocline is the upward tilting of the isopycnals at the coast and over the shelf region. This is forced by the intensification of the alongshore winds and the positive wind-stress curl during spring and part of the summer. In the previous section we also verified that the ocean response also involves westward propagation that can be explained through quasi-linear Rossby wave dynamics in the region of the continental slope and deeper ocean.

To describe succinctly the spatial and temporal evolution of the seasonal circulation and wind forcing over the shelf region, we linearly decompose the density surface (26.5) depth anomaly ( $\Delta h$ ) and the wind-stress curl anomaly using empirical orthogonal functions (EOFs). Fig. 10 shows the spatial pattern and the temporal amplitudes for the first two modes which together account for more than 95% of the seasonal variance (80–85% for first mode and 10–14% for the second).

The first mode of  $\Delta h$  shows a region of strong negative anomaly (low) over the northern part of

the shelf region (Fig. 10a, color bars are not the same in each panel). Negative anomalies indicate an upward tilting of the density surface, so that the low is interpreted as an intensification of cyclonic circulation. This intensification is clearly associated with the input of relative vorticity by the anomalous positive wind-stress curl (Fig. 10b) through Ekman Pumping, as previously verified in the linearized model. The intensification of one cyclonic gyre as it appears in the first mode is rarely observed in synoptic maps of the ocean model circulation. The increase in relative vorticity of the currents does not spatially match the smooth pattern of the positive wind-stress curl used to force the model because of the geometrical constraints of islands and sudden changes in the topography that affect the flow field. In the real ocean non-seasonal winds introduce even more ambiguity in identifying a clear closed cyclonic gyre intensification in the observations. This explains why the SCE is a feature that is strongly evident in the mean but is hardly ever observed in a synoptic map.

Observations show that the SCE has a seasonal peak toward early summer (Lynn and Simpson, 1987). The temporal evolution of the first modes of  $\Delta h$  (Fig. 10c) and the anomalous wind-stress curl (Fig. 10f) also show a peak towards early summer and are strongly correlated.

In the second mode we find an inshore/offshore dipole in the ocean  $\Delta h$  anomalies (Fig. 10b). The sign of the mode is negative inshore and positive offshore during late winter and spring as seen in the temporal evolution of the amplitude (Fig. 10c). Towards summer the amplitude of the mode switches sign sharply to positive. The maximum of the positive phase is reached in the summer and then decays towards negative values during the end of fall. A physical interpretation is as follows: during early spring the upwelling winds (associated with positive wind curl at the coast) force equatorward flow along the coast (associated with negative  $\Delta h$  at the coast). Toward summer the anomalous wind-stress curl at the coast becomes negative and intensifies poleward flow in the bight (positive  $\Delta h$  at the coast). It is important to notice that the mode 2 principal component of wind (Fig. 10f) leads that of the ocean during winter and

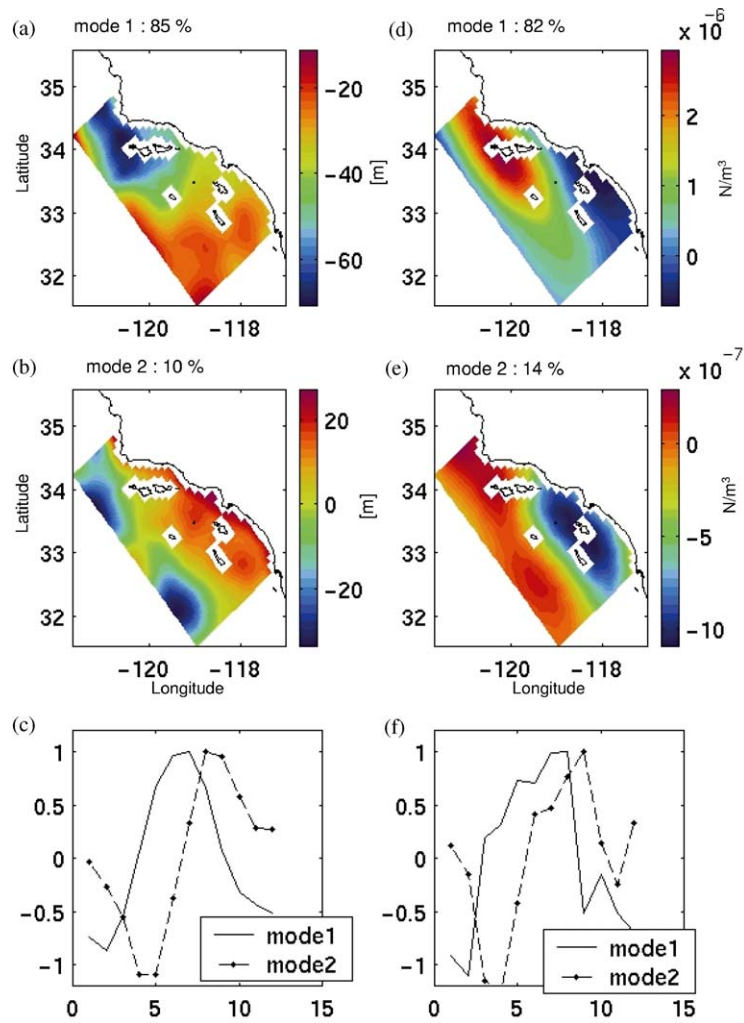


Fig. 10. Empirical orthogonal functions: Mode 1 (a) and Mode 2 (b) for the 26.5 isopycnal depth, and their temporal amplitudes (c). Mode 1 (d) and Mode 2 (e) for the RSM wind-stress curl and their temporal amplitudes (f).

spring but lags during late summer. This is the signature of the offshore propagation of the  $\Delta h$  anomaly associated with Rossby dynamics, which acts on a time scale faster than the wind-stress curl anomaly reversal.

### 6. Conclusions

A numerical ocean simulation that uses down-scaled winds from a regional atmospheric model (case RSM) as surface forcing is successful in

capturing the mean and seasonal circulation in the SCCS as observed in the CalCOFI in situ long-term hydrographic data. The seasonal cycle in the model is characterized by an annually recurrent westward propagation of a negative isopycnal depth anomaly that develops over the entire continental shelf during upwelling favorable winds in spring and summer. Sensitivity analysis of the ocean model to different wind forcing, including large-scale analyses and downscaled products, reveals that the spatial and temporal signature of these anomalies depends strongly on the details of

wind stress and its curl. A linearized version of the model, which only includes the long-wave response of the oceanic system, shows that quasi-linear Rossby wave dynamics explains a significant fraction of the variance (up to 80%) associated with the westward propagation in the non-linear model. The explained variance is higher in the near-shore regions where the circulation responds more linearly to changes in the forcing, as confirmed by a distinct seasonal peak in the energy spectra of SSH anomalies. Farther offshore this peak is not as clear and the spectral energy spreads over a broader range of frequencies. In this region, referred as the mesoscale *eddy field zone*, the linearized model explains a smaller fraction of the variance (about 40%) and other processes such as baroclinic and barotropic instabilities become important dynamical elements.

A conceptual dynamical framework that summarizes the relationship between the winds and the seasonal circulation in the Southern California Current System as deduced from the observational and ocean model analysis is as follows:

- (1) In spring, strong upwelling winds along the coast generate an upward tilt of the isopycnals in the Bight, thereby developing a negative anomaly ( $\Delta h$ ) of the density surface (Fig. 11a) and southward flow along the coast in the Bight.
- (2) As the spring transitions to the summer (Fig. 11b) the upwelling winds relax in the Bight, but are still strong further offshore over the continental slope (positive winds stress curl in the SCB). Adjustment of the anomalously dense waters in the coastal upwelling region initiates a westward displacement of the ocean density anomaly. Coastal poleward flow develops as the density anomaly progresses westward over the shelf region.
- (3) The shoaling of isopycnals over the northern part of the shelf is reinforced by Ekman pumping (11b). The combined action of the wind-stress curl and the coastal deflection of the poleward flow generate positive relative vorticity (reinforcing cyclonic recirculation) in early summer. This is historically referred to in the literature as the Southern California Eddy

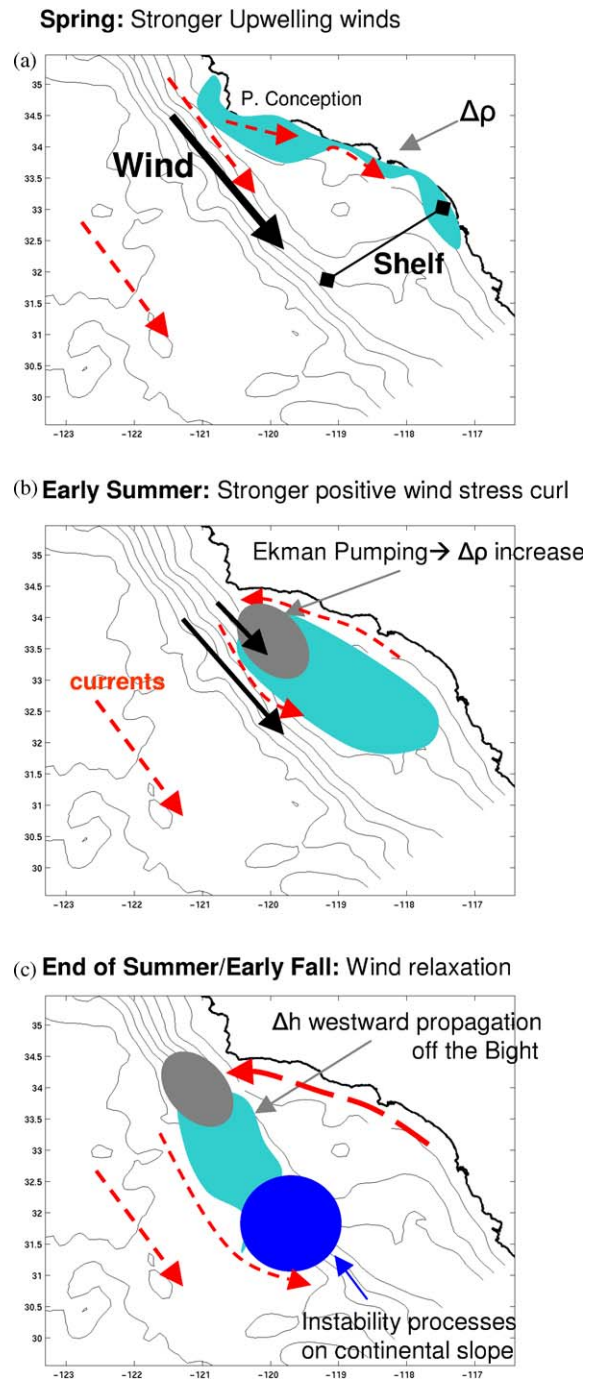


Fig. 11. Schematic of the seasonal dynamics in the Southern California Current System for spring (a), early summer (b), and fall (c). Black arrows are wind stress, red arrows are current and shaded areas denote areas of shoaling of isopycnal depths (positive density anomaly).

in the northern part of the shelf. Because of the geometry of the domain (coastline, topography, and islands in particular), the relative vorticity of the flow is not spatially uniform as the density anomaly and a closed cyclonic eddy is hardly ever observed in individual synoptic maps of the ocean.

- (4) As summer progresses, the westward propagation of the  $\Delta h$  anomaly over the entire SCB region continues further offshore while along the coast poleward flow intensifies. The intensification and dynamics of the poleward flow has not been addressed explicitly in this study. However, our results corroborate previous work which suggests that poleward flow along the coast requires positive wind-stress curl (Oey, 1999).
- (5) Towards the end of summer the recirculation region is broader and becomes increasingly unstable as the core of the ocean  $\Delta h$  anomaly crosses the continental slope (Fig. 11c). Instability processes, characterized by barotropic and baroclinic energy conversion terms of comparable amplitude (not shown in the figures), are a generating mechanism for eddies

at this point of the seasonal cycle. These eddies are commonly found in observations and are a robust feature in the numerical model. Their signature is also found in the model EKE (Fig. 12), which reaches a seasonal maximum at the end the summer in the cyclonic recirculation region (over the continental slope where the instabilities develop) and in late fall further offshore where the eddies are fully developed. A careful look at an animation of the model SSH anomaly (<http://horizon.ucsd.edu/movies/rsm-dssh.gif>) confirms this view of the seasonal cycle in the surface EKE and shows the complicated evolution of the generated eddies.

### Acknowledgements

I gratefully acknowledge funding from NASA (NAG5-6497 and NAG5-9788), ONR (N00014-99-1-0045) and NOAA (through the Experimental Climate Prediction Center, NA77RJ0453). The views expressed herein are those of the authors and do not necessarily reflect the views of NOAA or any of its sub-agencies. Supercomputing resources were additionally provided by the San Diego Supercomputer Center and NASA. We thank our colleagues at Rutgers University (Hernan Arango, Kate Hedstrom and Dale Haidvogel) and UCLA (Sasha Shchepetkin, Patrick Marchesiello and Jim McWilliams) for generously allowing use of their computer models and aiding in many aspects of this work. We also thank our CalCOFI colleagues (Teri Chereskin, Peter Niiler, Ron Lynn, Douglas Neilson, and Tom Hayward) for providing data in accessible form and for many important discussions. Special thanks to Jack Ritchie for running the atmospheric Regional Spectral Model; and to Arthur Miller for the scientific discussions and advice during the preparation of the manuscript.

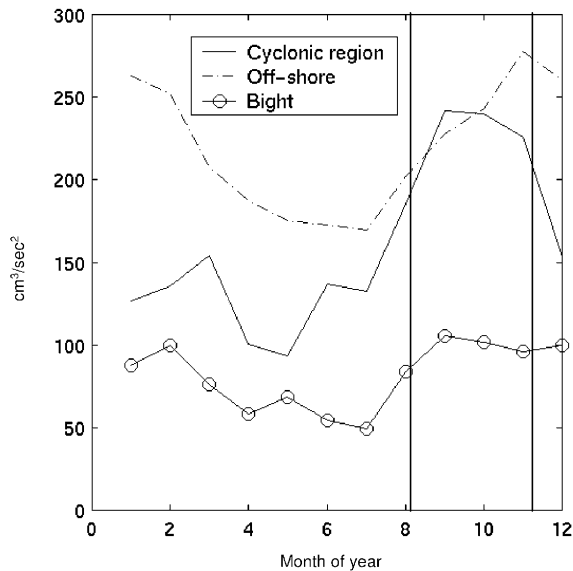


Fig. 12. Model Eddy Kinetic Energy integrated over different domains: the Bight region (solid line with circles), the cyclonic recirculation region (solid line), and the deep ocean off the continental slope (dashed line).

### References

- Allen, J.S., 1980. Models of wind-driven currents on the continental-shelf. *Annual Review of Fluid Mechanics* 12, 389–433.

- Auad, G., Paressierra, A., Vallis, G.K., 1991. Circulation and energetics of a model of the California Current System. *Journal of Physical Oceanography* 21 (10), 1534–1552.
- Bakun, A., Nelson, C.S., 1991. The seasonal cycle of wind-stress curl in subtropical eastern boundary current regions. *Journal of Physical Oceanography* 21, 1815–1834.
- Batteen, M.L., 1997. Wind-forced modeling studies of currents, meanders, and eddies in the California Current System. *Journal of Geophysical Research—Oceans* 102 (C1), 985–1010.
- Bograd, S.J., Digiaco, P.M., Durazo, R., Hayward, T.L., Hyrenbach, K.D., Lynn, R.J., Mantyla, A.W., Schwing, F.B., Sydeman, W.J., Baumgartner, T., Lavanigos, B., Moore, C.S., 2000. The state of the California Current, 1999–2000: forward to a new regime? California Cooperative Oceanic Fisheries Investigations Reports 41, 26–52.
- Bray, N.A., Keyes, A., Morawitz, W.M.L., 1999. The California Current system in the Southern California Bight and the Santa Barbara channel. *Journal of Geophysical Research—Oceans* 104 (C4), 7695–7714.
- Chereskin, T.K., Trunnell, M., 1996. Correlation scales, objective mapping, and absolute geostrophic flow in the California Current. *Journal of Geophysical Research—Oceans* 101 (C10), 22619–22629.
- da Silva, A., Young, C., Levitus, S., 1994. Atlas of Surface Marine Data 1994. NOAA Atlas NESDIS 6-10, US Government Printing Office, Washington, DC, pp. 1–5.
- Di Lorenzo, E., Miller, A.J., Neilson, D.J., Cornuelle, B.D., Moisan, J.R., 2003. Modeling observed California Current mesoscale eddies and the ecosystem response. *International Journal of Remote Sensing*, in press.
- Haidvogel, D.B., Beckmann, A., Hedstrom, K.S., 1991. Dynamic simulations of filament formation and evolution in the coastal transition zone. *Journal of Geophysical Research—Oceans* 96 (C8), 15017–15040.
- Hayward, T.L., Mantyla, A.W., Lynn, R.J., Smith, P.E., Chereskin, T.K., 1994. The State of the California Current in 1993–1994. California Cooperative Oceanic Fisheries Investigations Reports 35, 19–835.
- Hickey, B.M., 1992. Circulation over the Santa-Monica San-Pedro Basin and Shelf. *Progress in Oceanography* 30 (1–4), 37–115.
- Hickey, B.M., 1998. Coastal oceanography of western North America from the tip of Baja California to Vancouver Island. In: Robinson, A.R., Brink, K.H. (Eds.), *Coastal Segment, The Sea*, Vol. 11. Wiley, New York, pp. 345–391.
- Kelly, K.A., Beardsley, R.C., Limeburner, R., Brink, K.H., Paduan, J.D., Chereskin, T.K., 1998. Variability of the near-surface eddy kinetic energy in the California Current based on altimetric, drifter, and moored current data. *Journal of Geophysical Research—Oceans* 103 (C6), 13067–13083.
- Kelly, K.A., Caruso, M.J., Austin, J.A., 1993. Wind-forced variations in sea-surface height in the Northeast Pacific-Ocean. *Journal of Physical Oceanography* 23 (11), 2392–2411.
- Large, W.G., McWilliams, J.C., Doney, S.C., 1994. Oceanic vertical mixing—a review and a model with a nonlocal boundary-layer parameterization. *Reviews of Geophysics* 32 (4), 363–403.
- Levitus, S., Burgett, R., Boyer, T.P., 1994. World Ocean Atlas 1994. NOAA Atlas NESDIS 4, US Government Printing Office, Washington, DC, pp. 3–4.
- Lynn, R.J., Simpson, J.J., 1987. The California Current System—the seasonal variability of its physical characteristics. *Journal of Geophysical Research—Oceans* 92(C12), 12947–12966.
- Marchesiello, P., McWilliams, J.C., Shchepetkin, A., 2001. Open boundary conditions for long-term integration of regional oceanic models. *Ocean Modelling* 3, 1–20.
- Marchesiello, P., McWilliams, J.C., Shchepetkin, A., 2003. Equilibrium structure and dynamics of the California Current System. *Journal of Physical Oceanography* 33 (4), 753–783.
- McCreary, J.P., Kundu, P.K., Chao, S.Y., 1987. On the dynamics of the California Current System. *Journal of Marine Research* 45 (1), 1–32.
- Mied, R.P., McWilliams, J.C., Lindemann, G.J., 1991. The Generation and evolution of mushroom-like vortices. *Journal of Physical Oceanography* 21 (4), 489–510.
- Miller, A.J., McWilliams, J.C., Schneider, N., Allen, J.S., Barth, J.A., Beardsley, R.C., Chavez, F.P., Chereskin, T.K., Edwards, C.A., Haney, R.L., Kelly, K.A., Kindle, J.C., Ly, L.N., Moisan, J.R., Noble, M.A., Niiler, P.P., Oey, L.Y., Schwing, F.B., Shearman, R.K., Swenson, M.S., 1999. Observing and modeling the California Current System. *Eos Transactions—American Geophysical Union* 80, 533–539.
- NGDC, 1998. Digital relief of the surface of the Earth. NOAA, National Geophysics Data Center, Boulder, CO (Data announcement 88-MG-02).
- Oey, L.Y., 1999. A forcing mechanism for the poleward flow off the southern California coast. *Journal of Geophysical Research—Oceans* 104 (C6), 13529–13539.
- Paressierra, A., O'Brien, J.J., 1989. The seasonal and inter-annual variability of the California Current System—a numerical-model. *Journal of Geophysical Research—Oceans* 94 (C3), 3159–3180.
- Paressierra, A., White, W.B., Tai, C.K., 1993. Wind-driven coastal generation of annual mesoscale eddy activity in the California Current. *Journal of Physical Oceanography* 23 (6), 1110–1121.
- Schwartzlose, R.A., 1963. Nearshore currents of the Western United States and Baja California as measured by drift bottles. California Cooperative Oceanic Fisheries Investigation Progress Report, 7-1-60 to 6-3-62, Marine Research Committee, California Department of Fish and Game, Sacramento, CA, pp. 15–22.
- Shchepetkin, A., McWilliams, J.C., 1998. Quasi-monotone advection schemes based on explicit locally adaptive dissipation. *Monthly Weather Review* 126 (6), 1541–1580.
- Shchepetkin, A., McWilliams, J.C., 2003. A method for computing horizontal pressure-gradient force in an oceanic

- model with a non-aligned vertical coordinate. *Journal of Geophysical Research—Oceans* 108 (C3), in press.
- Simpson, J.J., Lynn, R.J., 1990. A mesoscale eddy dipole in the offshore California Current. *Journal of Geophysical Research—Oceans* 95 (C8), 13009–13022.
- Song, Y.H., Haidvogel, D., 1994. A semiimplicit ocean circulation model using a generalized topography—following coordinate system. *Journal of Computational Physics* 115 (1), 228–244.
- Strub, P.T., James, C., 2000. Altimeter-derived variability of surface velocities in the California Current System: 2. Seasonal circulation and eddy statistics. *Deep-Sea Research Part II* 47 (5–6), 831–870.
- Strub, P.T., Kosro, P.M., Huyer, A., 1991. The Nature of the Cold Filaments in the California Current System. *Journal of Geophysical Research—Oceans* 96 (C8), 14743–14768.
- Sverdrup, H.U., Fleming, R.H., 1941. The waters off the coast of southern California. *Scripps Institute of Oceanography Bulletin* (4), 261–387.
- Swenson, M.S., Niiler, P.P., 1996. Statistical analysis of the surface circulation of the California Current. *Journal of Geophysical Research—Oceans* 101 (C10), 22631–22645.
- Winant, C.D., Dorman, C.E., 1997. Seasonal patterns of surface wind stress and heat flux over the Southern California Bight. *Journal of Geophysical Research—Oceans* 102 (C3), 5641–5653.